Supporting Information

Tailoring Co-Doping of Cobalt and Nitrogen in Fullerene-Based Carbon Composite and Its Effect for Supercapacitive Performance

Bohong Jiang,[a#] Guangpu Zhang,[b#] Qin Tang,[c] Fancang Meng,[a] Dechun Zhou,[a] Wenli Zhao,[a] Wei Jiang,[b*] Qingmin, Ji[a*]

[a] *Herbert Gleiter Institute for Nanoscience, School of Materials Science and Engineering, Nanjing University of Science & Technology, 200 Xiaolingwei, Nanjing, 210094, China*

[b] *National Special Superfine Powder Engineering Technology Research Center, Nanjing University of Science and Technology, 200 Xiaolingwei, Nanjing, 210094, China*

[c] *School of Chemistry and Chemical Engineering, Yancheng Institute of Technology, No. 1 Mid. Xiwang Avenue, Yancheng, China*

[#] These authors contributed equally to this work

*Corresponding author: jiqingmin@njust.edu.cn, superfine_jw@126.com

Additional Data

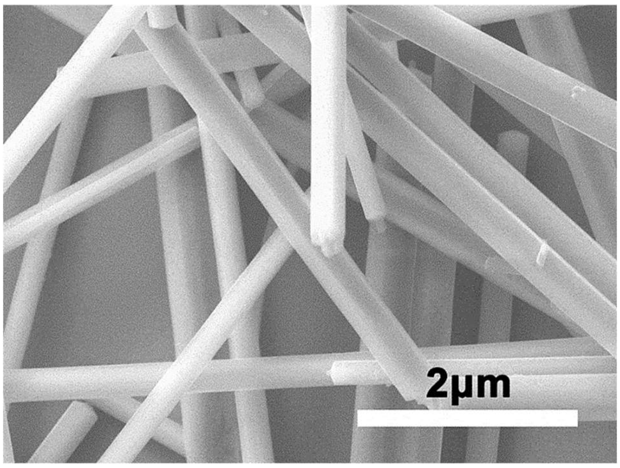

Fig. S1. SEM image of C_{60}-rods by LLIP process of C_{60}s in toluene-isopropyl alcohol solution.

Table S1. Structural features of C_{60} rods and C_{60}CoTMPP superstructures.

Sample	Morphology	Length (μm)	diameter (μm)
C_{60}-rod (assembled structure from bare)	Long rod	10	0.15-0.40
C_{60}CoTMPP-0.2	Short rods with polyprism structure	2.5	0.9
C_{60}CoTMPP-0.1	Microsphere with lamellar structures		1.9
C_{60}CoTMPP-0.05	Short rod	2.3	1.2

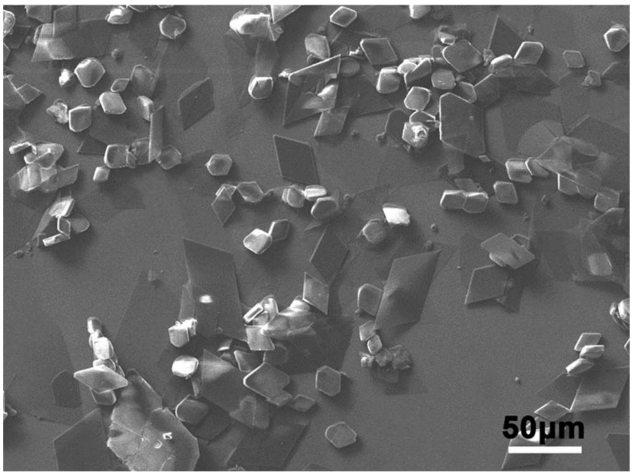

Fig. S2. SEM image of CoTMPP crystals formed in toluene-isopropyl alcohol solution.

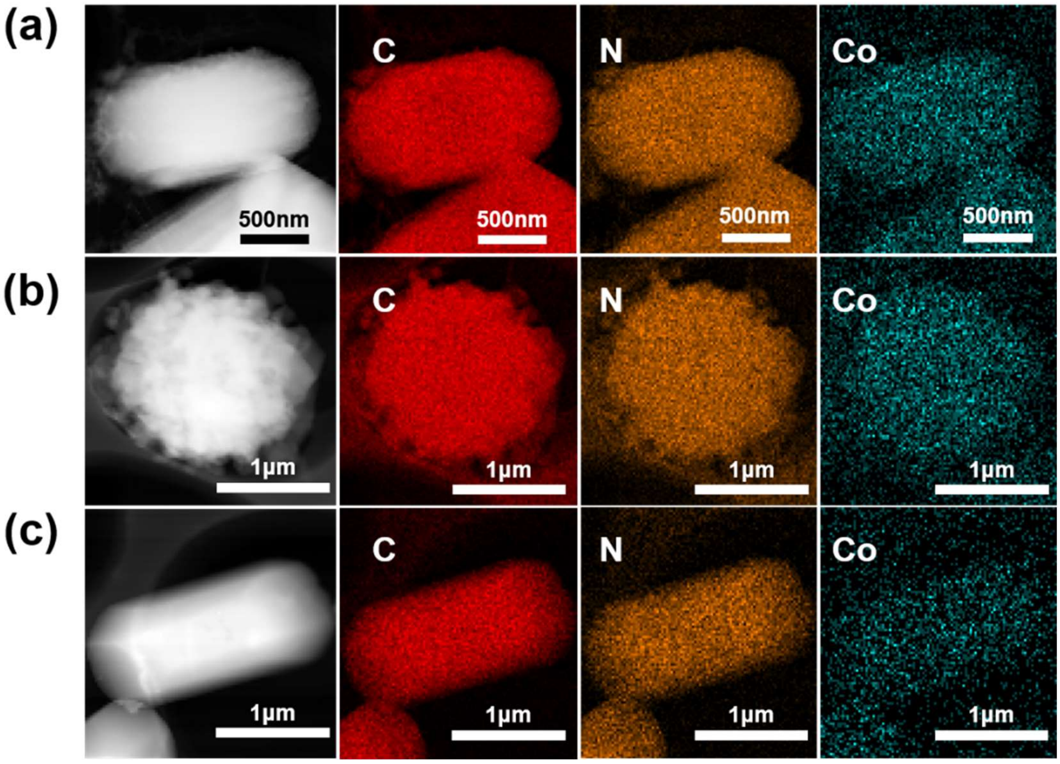

Fig. S3. STEM images and the corresponding elemental mapping images of C_{60}CoTMPP crystals. (a) C_{60}CoTMPP-0.2, (b) C_{60}CoTMPP-0.1, (c) C_{60}CoTMPP-0.05.

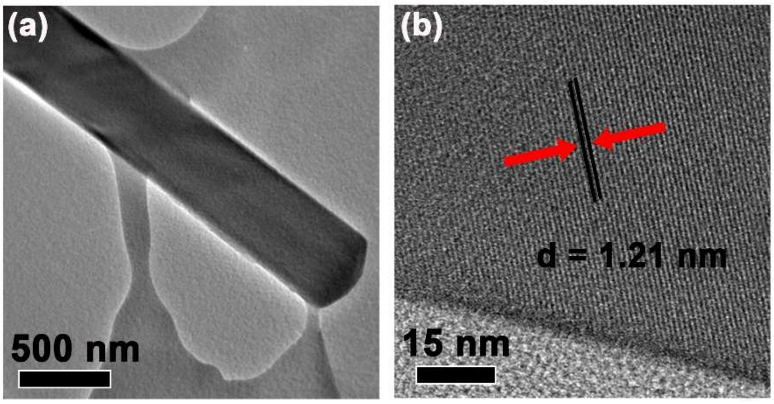

Fig. S4. TEM images of C_{60} rod without CoTMPPs.

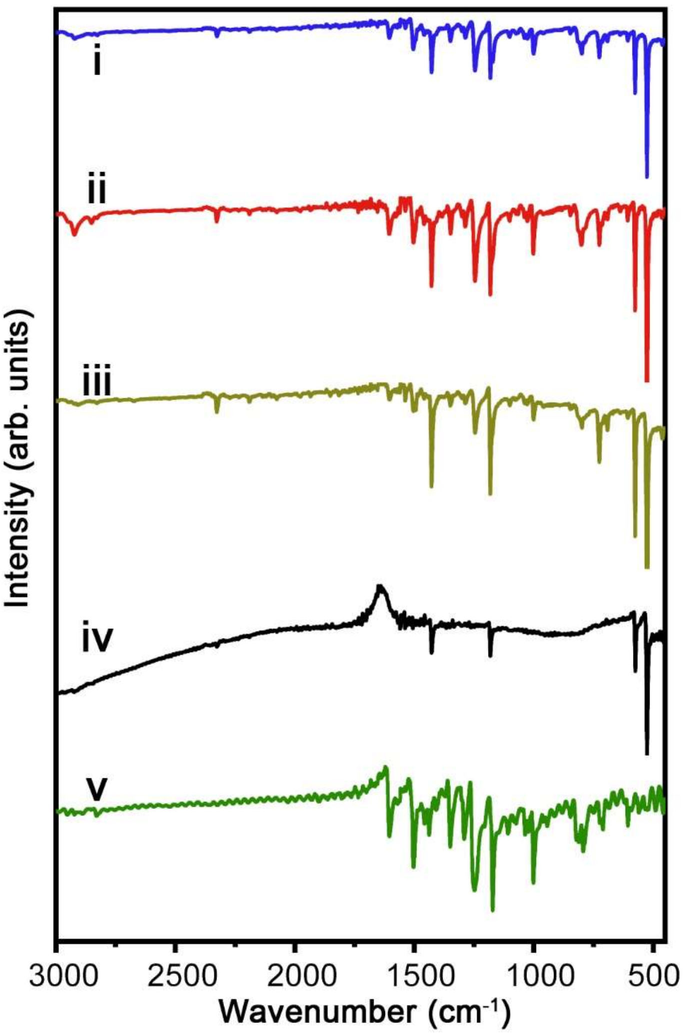

Fig. S5. FTIR spectra of C_{60}CoTMPP crystals and CoTMPP. (i) C_{60}CoTMPP-0.2, (ii) C_{60}CoTMPP-0.1, (iii) C_{60}CoTMPP-0.05, (iv) C_{60}-rods, and (v) CoTMPP.

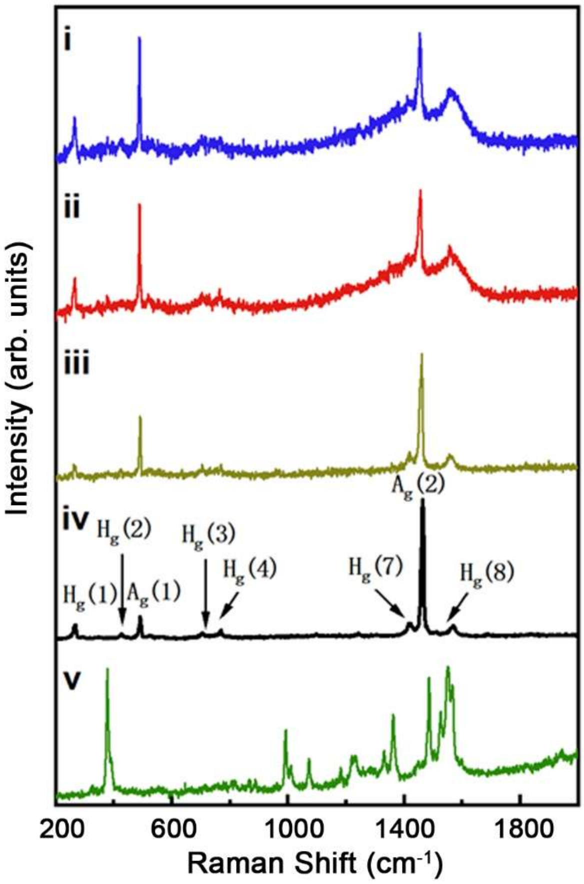

Fig. S6. Raman spectra of C_{60}CoTMPP superstructures and CoTMPPs. (i) C_{60}CoTMPP-0.2, (ii) C_{60}CoTMPP-0.1, (iii) C_{60}CoTMPP-0.05, (iv) C_{60}-rods, and (v) CoTMPP.

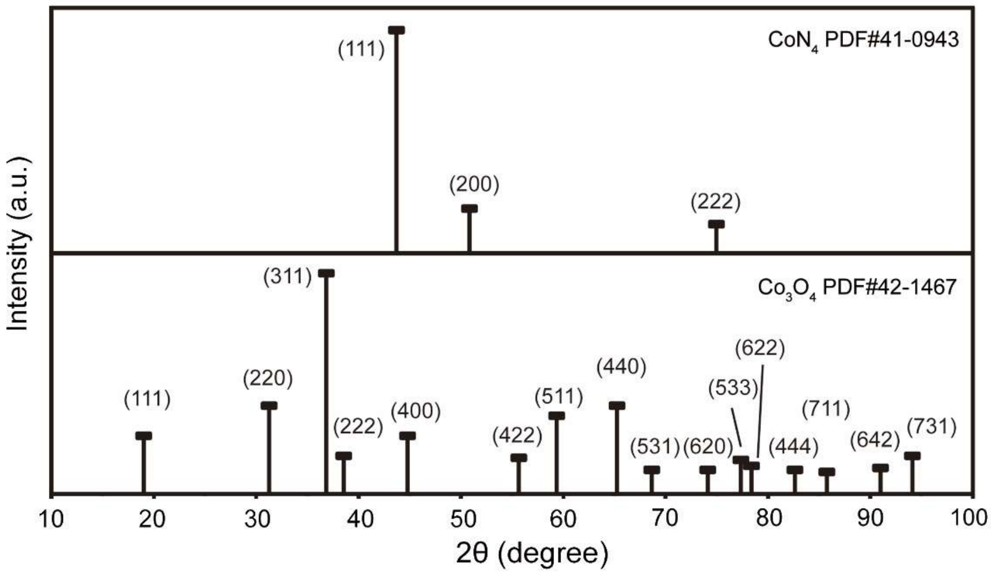

Fig. S7. XRD patterns of CoN_4 and Co_3O_4 standard cards.

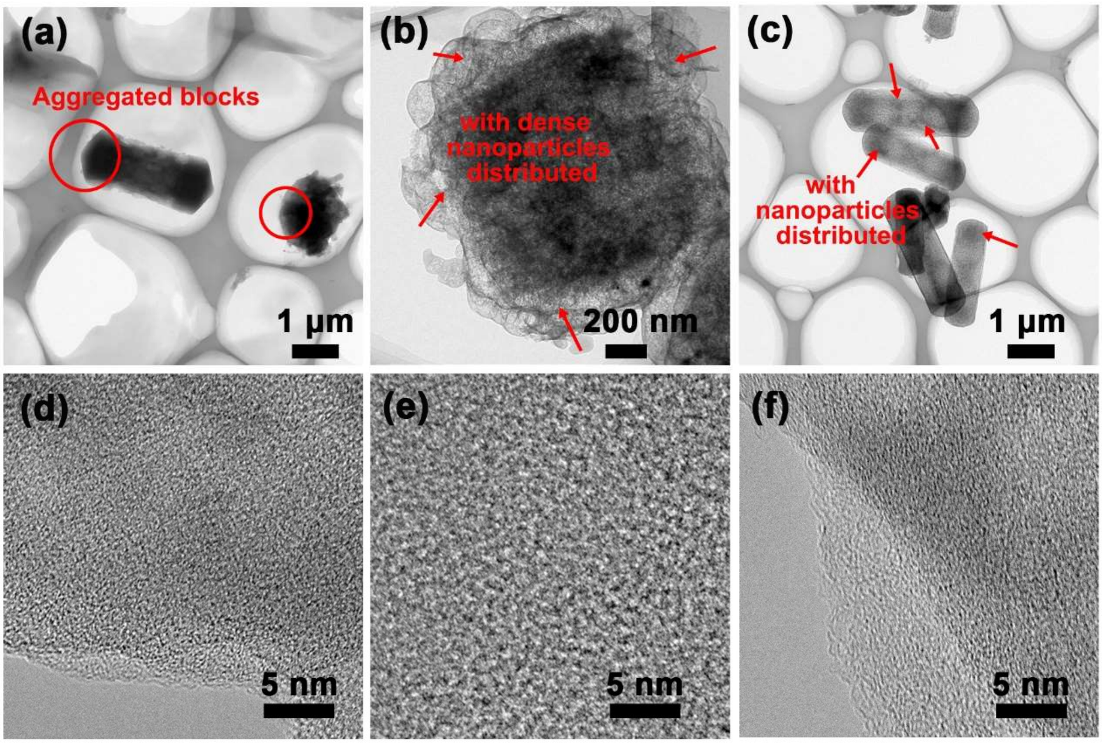

Fig. S8. TEM images of C_{60}CoTMPP_900s. (a), (d) C_{60}CoTMPP-0.2_900; (b), (e) C_{60}CoTMPP-0.1_900; (c), (f) C_{60}CoTMPP-0.05_900.

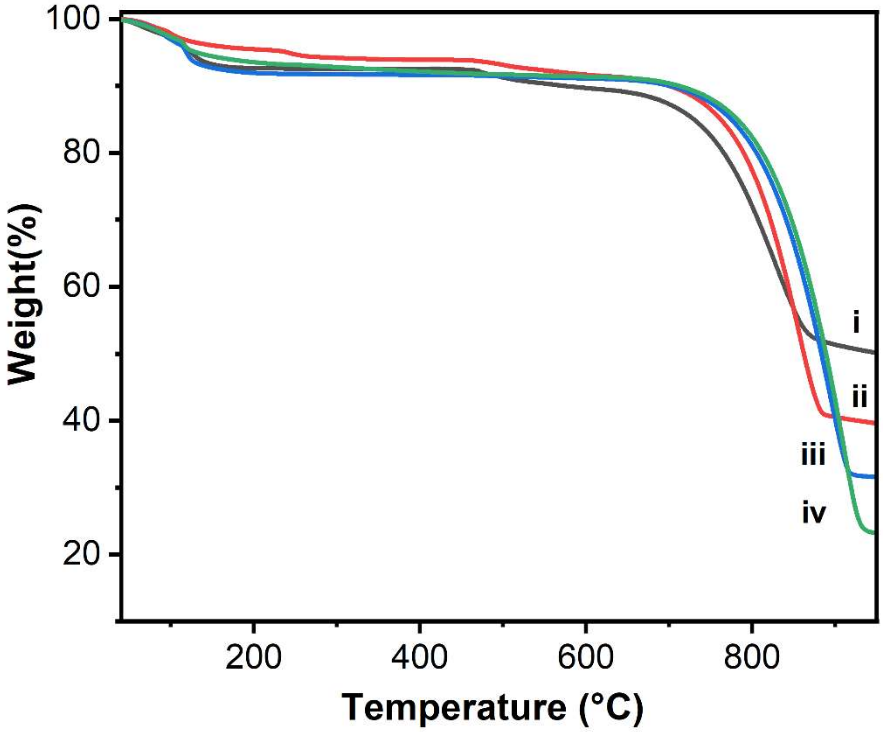

Fig. S9. The TGA weight loss curves of C_{60}CoTMPPs. (i) C_{60}CoTMPP-0.2, (ii) C_{60}CoTMPP-0.1, (iii) C_{60}CoTMPP-0.05, (iv) C_{60}-rods.

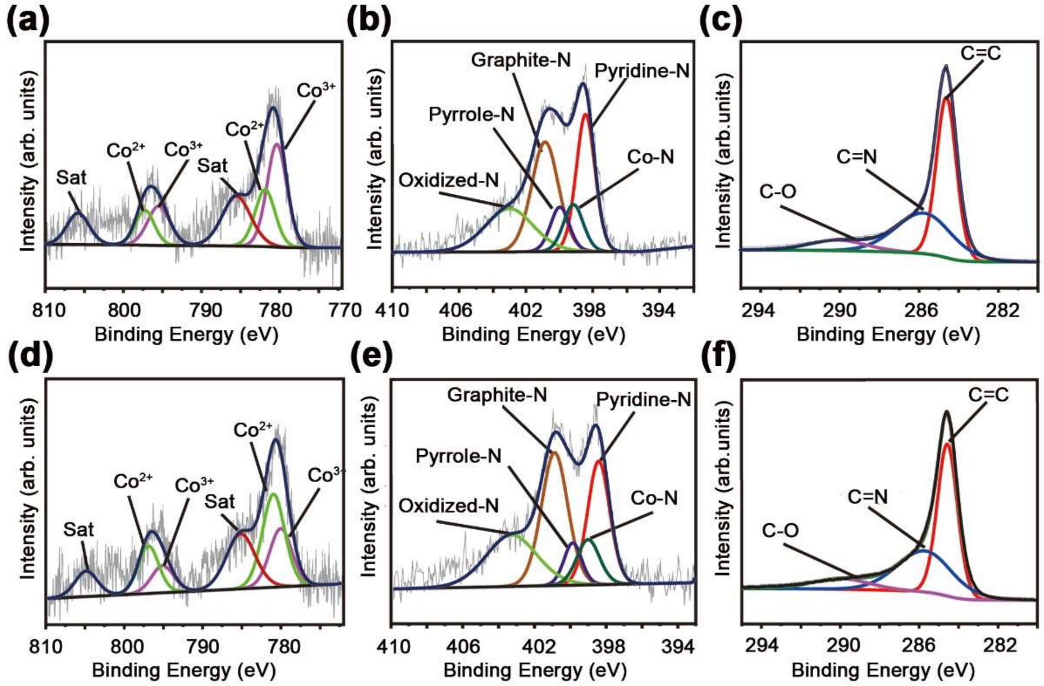

Fig. S10. (a) XPS Co 2p spectrum, (b) XPS N 1s spectrum, (c) XPS C 1s spectrum of C_{60}CoTMPP-0.2_900; (d) XPS Co 2p spectrum (e) XPS N 1s spectrum, (f) XPS C 1s spectrum of C_{60}CoTMPP-0.05_900.

Table S2. The comparison for the proportion of Co^{2+} and Co^{3+} in C_{60}CoTMPP_900s based on the relative area of each component peak in XPS Co 2p spectra, and the proportion of pyridine-N and Co-N in C_{60}CoTMPP_900s based on the relative area of each component peak in XPS N 1s spectra.

Samples	Co^{3+}	Co^{2+}	Pyridine-N	Co-N
C_{60}CoTMPP-0.2_900	44.24%	24.77%	27.35%	10.01%
C_{60}CoTMPP-0.1_900	24.51%	49.86%	26.49%	31.85%
C_{60}CoTMPP-0.05_900	26.24%	41.86%	25.53%	7.31%

Table S3. The Co amounts in C_{60}CoTMPPs and C_{60}CoTMPP_900s by ICP measurements.

Samples	C_{60}CoTMPP -0.05	C_{60}CoTMPP -0.1	C_{60}CoTMPP -0.2	C_{60}CoTMPP -0.05_900	C_{60}CoTMPP -0.1_900	C_{60}CoTMPP -0.2_900
Co mass% by ICP	0.26	0.57	1.26	0.30	0.71	1.52
Theoretical Co mass%	0.38	0.73	1.34	-	-	-

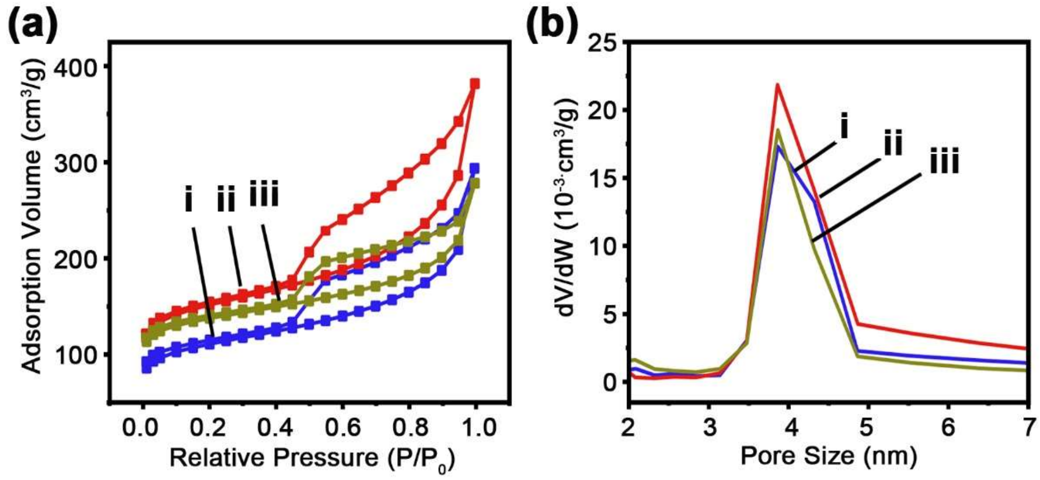

Fig. S11. (a) Nitrogen isotherms and (b) pore size distributions of the C_{60}CoTMPP_900s (i) C_{60}CoTMPP-0.2_900, (ii) C_{60}CoTMPP-0.1_900, (iii) C_{60}CoTMPP-0.05_900.

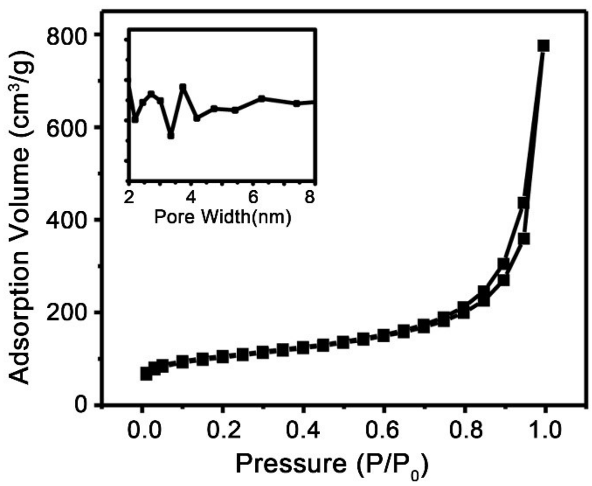

Fig. S12. Nitrogen isotherms and pore size distribution (inset) of the C_{60} _900 (rod morphology).

Table S4. The porous features of C_{60}_900 and various C_{60}CoTMPP_900s.

Sample	BET surface area (m^2/g)	Average Pore size (nm)	Pore volume (cm^3/g)
C_{60}_900	287	2.3	0.059
C_{60}CoTMPP-0.2_900	365	3.9	0.094
C_{60}CoTMPP-0.1_900	496	3.9	0.143
C_{60}CoTMPP-0.05_900	446	3.9	0.142

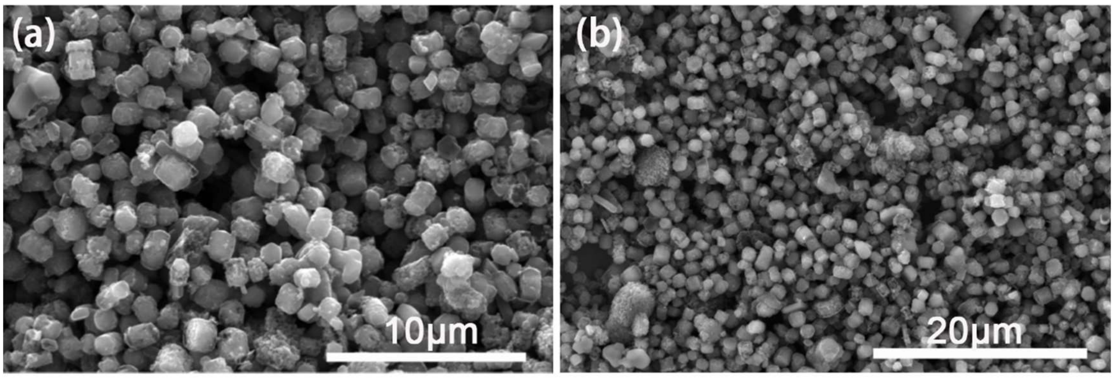

Fig. S13. SEM images of the C_{60}CoTMPP-0.1_900 on the electrode surface.

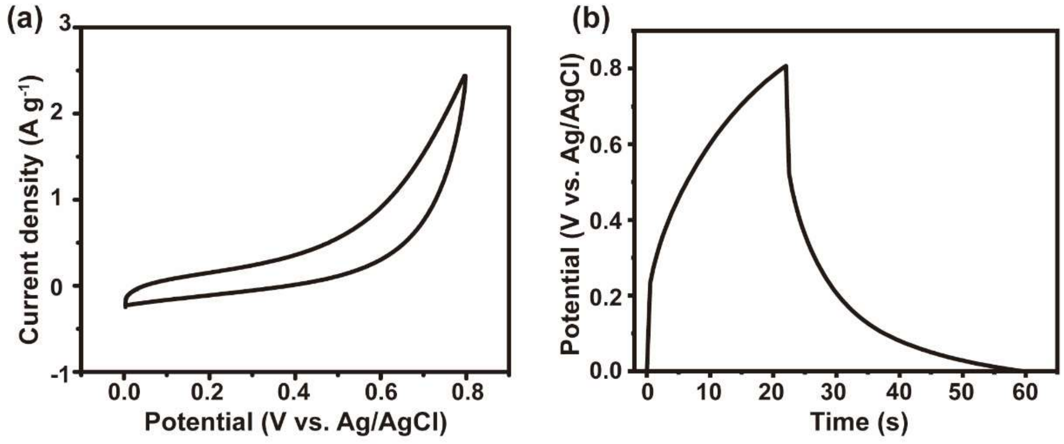

Fig. S14. (a) CV curve of C_{60}_900 at the scan rate of 10 mV·s^{-1}, (b) CD curve of C_{60}_900 at 1A·g^{-1}.

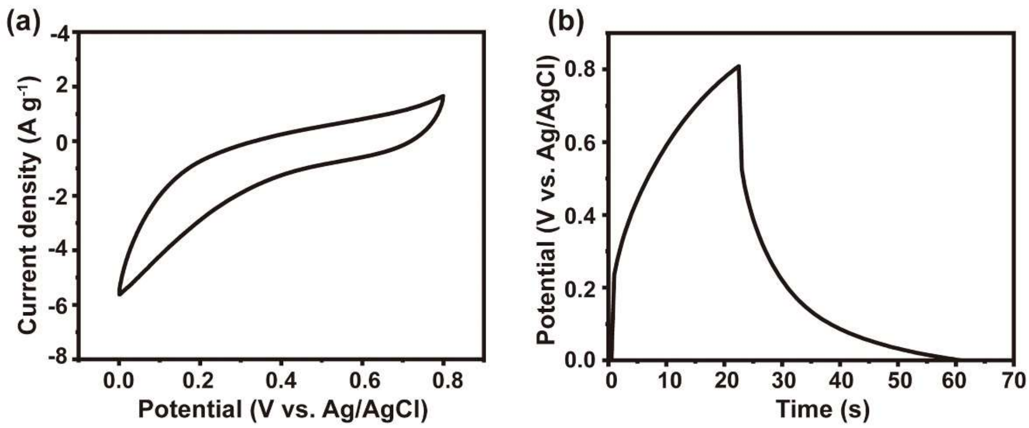

Fig. S15. (a) CV curve of C_{60}CoTMPP-0.1_700 at the scan rate of 10 mV·s^{-1}, (b) CD curve of C_{60}CoTMPP-0.1_700 at 1A·g^{-1}.

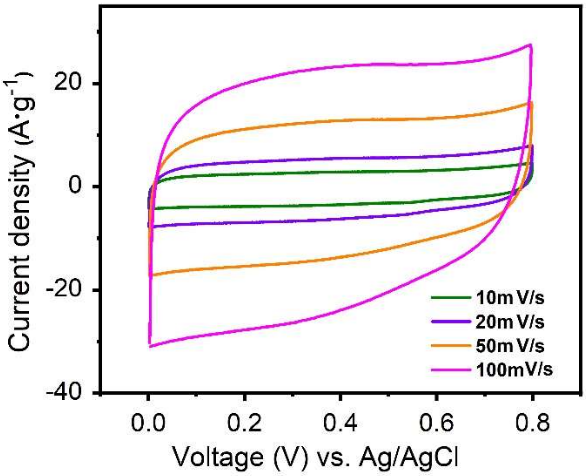

Fig. S16. CV curves of C_{60}CoTMPP-0.1_900 at different scan rates (10–100 mV·s^{-1}).

Table S5. The comparison of the supercapacitor performance with various reported fullerene-derived carbon materials.

Materials	**CD**		**CV**		Ref.
	(F/g)	(A/g)	(F/g)	(mA/s)	
C_{60} nanosheet	-	-	12.7	5	1
MF C_{60}	141	0.5	-	-	2
HT-FNT_2000(C_{60})	-	-	145	5	3
HT-FNR_2000(C_{60})	-	-	132	5	3
Fe-MFC_{60}-150	112.4	0.1	-	-	4
FCL700 (C_{60})	505.4	0.1	-	-	5
MCFC-900 (C_{70})	205	1	286	5	6
HTFT_2000(C_{70})	-	-	212	5	6
HTFT_900(C_{70})	-	-	26.4	5	7
MC_{60}@C-1.33	213	0.5			8
200-HTC-800			2995	40	9
C_{60}FcC_{60}-8IPA_900	129	1	102.5	10	10
C_{60}CoTMPP-0.1_900	416.31	1	296	10	this work

References (in Table S5)

1. L. K. Shrestha, Y. Yamauchi, J. P. Hill, K. Miyazawa, K. Ariga, *J. Am. Chem. Soc.*, 2013, **135**, 586-589.

2. M. Benzigar, S. Joseph, H. Ilbeygi, D. H. Park, S. Sarkar, G. Chandra, S. Umapathy, S. Srinivasan, S. Talapaneni, A. Vinu, *Angew. Chem. Int. Edit.*, 2018, **57**, 569-573.

3. L. K. Shrestha, R. G. Shrestha, Y. Yamauchi, J. P. Hill, T. Nishimura, K.

Miyazawa, T. Kawai, S. Okada, K. Wakabayashi, K. Ariga, *Angew. Chem. Int. Edit.*, 2015, **54**, 951-955.

4. M. R. Benzigar, S. Joseph, G. Saianand, A. I. Gopalan, A. Vinu, *Micropor. Mesopor. Mat*, 2019, **285**, 21-31.
5. Z. Peng, Y. Hu, J. Wang, S. Liu, C. Li, Q. Jiang, J. Lu, X. Zeng, P. Peng, F. F. Li, *Adv. Energy Mater.,* 2019, **9**, 1802928.
6. P. Bairi, S. Maji, J. P. Hill, J. H. Kim, K. Ariga, L. K. Shrestha, *J. Mater. Chem. A.,* 2019, **7**, 12654-12660.
7. P. Bairi, R. G. Shrestha, J. P. Hill, T. Nishimura, K. Ariga, L.K. Shrestha, *J. Mater. Chem. A.*, 2016, **4**, 13899-13906.
8. A. V. Baskar, A. M. Ruban, J. M. Davidraj, G. Singh, A. H. Al-Muhtaseb, J. M. Lee, J. Yi, A. Vinu, *Bull. Chem. Soc. Jpn.*, 2021, **94**, 133-140.
9. Y. Wu, J.-P. Cao, X.-Y. Zhao, Z.-Q. Hao, Q.-Q. Zhuang, J.-S. Zhu, X.-Y. Wang, X.-Y. Wei, *Acta*, 2017, **252**, 397-407.
10. B. Jiang, Q. Tang, W. Zhao, J. Sun, R. An, T. Niu, H. Fuchs, Q. Ji, *CrystEngComm*, 2020, **22**, 6287-6294.